

Transverse component of the magnetic field in the solar photosphere observed by Sunrise

S. DANILOVIC,¹ B. BEECK,¹ A. PIETARILA,¹ M. SCHÜSSLER,¹ S. K. SOLANKI,^{1,7}
V. MARTÍNEZ PILLET,² J. A. BONET,² J. C. DEL TORO INIESTA,⁴ V. DOMINGO,⁵
P. BARTHOL,¹ T. BERKEFELD,³ A. GANDORFER,¹ M. KNÖLKER,⁶ W. SCHMIDT,³ &
A. M. TITLE⁸

¹Max-Planck-Institut für Sonnensystemforschung, Max-Planck-Str. 2, 37191
Katlenburg-Lindau, Germany.

²Instituto de Astrofísica de Canarias, C/Via Láctea s/n, 38200 La Laguna, Tenerife, Spain.

³Kiepenheuer-Institut für Sonnenphysik, Schöneckstr. 6, 79104 Freiburg, Germany.

⁴Instituto de Astrofísica de Andalucía (CSIC), Apartado de Correos 3004, 18080 Granada,
Spain.

⁵Grupo de Astronomía y Ciencias del Espacio, Universidad de Valencia, 46980 Paterna,
Valencia, Spain.

⁶High Altitude Observatory, National Center for Atmospheric Research, P.O. Box 3000,
Boulder CO 80307-3000, USA.

⁷School of Space Research, Kyung Hee University, Yongin, Gyeonggi, 446-701, Korea.

⁸Lockheed Martin Solar and Astrophysics Laboratory, Bldg. 252, 3251 Hanover Street,
Palo Alto, CA 94304, USA.

danilovic@mps.mpg.de

Received _____; accepted _____

ABSTRACT

We present the first observations of the transverse component of photospheric magnetic field acquired by the imaging magnetograph SUNRISE/IMaX. Using an automated detection method, we obtain statistical properties of 4536 features with significant linear polarization signal. We obtain a rate of occurrence of $7 \cdot 10^{-4} \text{ s}^{-1} \text{ arcsec}^{-2}$, which is 1 – 2 orders of magnitude larger than values reported by previous studies. We show that these features have no characteristic size or lifetime. They appear preferentially at granule boundaries with most of them being caught in downflow lanes at some point. Only a small percentage are entirely and constantly embedded in upflows (16%) or downflows (8%).

Subject headings: Sun: surface magnetism — Sun: granulation — techniques: polarimetric

1. Introduction

Recent observations with high spatial resolution and polarimetric sensitivity revealed that quiet photospheric regions contain a large amount of horizontal magnetic field (Orozco Suárez et al. 2007a,b; Lites et al. 2008). The size of the horizontal field patches varies from less than one to a few arcsec (Lites et al. 1996; De Pontieu 2002; Martínez González et al. 2007; Harvey et al. 2007; Ishikawa et al. 2008; Jin et al. 2009). Those with sizes comparable to the average size of the granular pattern are very dynamic (Ishikawa et al. 2008; Ishikawa & Tsuneta 2009; Jin et al. 2009). Such Horizontal Internetwork Fields (HIF) appear in internetwork as well as in plage regions with no significant difference in the rate of occurrence. Their lifetimes range from a minute to about ten minutes, comparable to the lifetime of granules. Some of them are recognized to be loop-like structures emerging cospatially with granules. They appear first inside the granule, then move to the intergranular lanes where they disappear (Centeno et al. 2007; Gömöry et al. 2010). Around 23% of such loop-like features rise and thus may contribute to the heating of higher atmospheric layers (Martínez González & Bellot Rubio 2009). On the other hand, some HIF are associated with downflows (Kubo et al. 2010).

MHD simulations show that horizontal magnetic field may appear during flux cancellations (Stein & Nordlund 2006) or flux emergence over single or multiple granules (Steiner et al. 2008; Cheung et al. 2007). Additionally, a significant amount of small-scale horizontal field is possibly produced through local dynamo action (Schüssler & Vögler 2008). To estimate what fraction of HIF has its origin in each of these processes could, however, be challenging since their observable signature may be similar.

Previous studies of HIF were based on slit observations of selected features that appear as single events, mostly associated with upflows. Here we use the first imaging observations obtained with the Imaging Magnetograph eXperiment (IMaX, Martínez Pillet et al.

2004; Martínez Pillet et al. 2010) onboard SUNRISE, a balloon-borne solar observatory (Barthol et al. 2010; Solanki et al. 2010; Berkefeld et al. 2010; Gandorfer et al. 2010), to obtain statistical properties of HIF. Mounted on a 1-m aperture telescope, IMaX provides two-dimensional maps of the vector magnetic field with exceptional spatial and temporal resolution. Using these data, we study all structures that show significant linear polarization signal in the selected quiet Sun time series. We examine their properties, in particular their connection with the velocity field.

2. Observations

We use two data sets obtained on June 9 2009, 00:36:02-00:58:46 UT (data set 1) and 01:30:54-02:02:29 UT (data set 2). The FOV covers $45'' \times 45''$ of a quiet region at disk center. Polarization maps were taken in 5 wavelength positions over the Fe I 525.02 nm line with a cadence of 33 s and a pixel size of $0.055''$. After data reduction (Martínez Pillet et al. 2010), two types of data are produced: non-reconstructed (level 1) and data reconstructed using phase-diversity information (level 2), reaching a spatial resolution of 0.15-0.18 arcsec. All data are corrected for instrumental effects, including intensity fluctuations due to interference fringes, dust particles, and illumination effects, as well as jitter-introduced polarization cross-talk, and blueshift over the FOV due to the collimated setup of the magnetograph etalon. The noise level of the non-reconstructed Stokes Q and U data is $\sim 10^{-3}I_c$. The reconstruction process amplifies the power of all spatial frequencies and, therefore, also increases the noise level by a factor of 2.5-3. Although the polarization signals are also amplified by the reconstruction, a significant amount is, nevertheless, lost in the noise. Thus, to identify the HIF we use the non-reconstructed linear polarization signal averaged over the 4 wavelength positions in the spectral line (Martínez Pillet et al. 2010, Eq. 15). To reduce the noise additionally, we applied the Gaussian filter with FWHM of 2

pixels ($0.11''$) to the linear polarization maps prior to the HIF identification.

3. Results

To obtain statistical properties of a large number of features with significant linear polarization signal, we use a modified version of the MLT (Multi Level Tracking) algorithm of Bovelet & Wiehr (2001) as an automatic detection method. MLT applies a sequence of thresholds with decreasing values to the mean linear polarization map. The algorithm identifies features when they show the largest signal and expands them in three dimensions (two spatial and one temporal) as the threshold value is decreased. After extensive tests we chose to use 13 thresholds ranging from $3.2 \cdot 10^{-3} I_c$ to a final threshold of $1.5 \cdot 10^{-3} I_c$. To avoid artificial splitting of structures with several intensity peaks we set an additional criterion. If two features were separate for threshold n and their maximum intensity does not exceed the $(n+1)$ th threshold value by more than 17.5%, we let them merge (Bharti et al. 2010). As an example, Fig. 1 shows a polarization map and the result of its MLT segmentation. The detected HIF have a wide range of sizes and appear to be organized on mesogranular scales.

3.1. Lifetime, size, and location

The total number of features that are followed in time and space from their appearance to their disappearance is 4536 (1911 in data set 1 and 2625 in data set 2). Taking into account that the features are detected during 22 min (data set 1) and 31 min (data set 2) in a FOV of $45'' \times 45''$, we obtain a rate of occurrence of $7.1 \cdot 10^{-4} \text{ s}^{-1} \text{ arcsec}^{-2}$ (data set 1) and $6.9 \cdot 10^{-4} \text{ s}^{-1} \text{ arcsec}^{-2}$ (data set 2). This is of 1-2 orders of magnitude higher than the values reported in previous studies (Lites et al. 1996; Ishikawa & Tsuneta 2009; Jin et al.

2009; Martínez González & Bellot Rubio 2009). The detected features occupy $\sim 3\%$ of the image area.

The distributions of lifetime and maximum area of the detected features are shown in Fig. 2a,b, respectively. Since the duration of the observations is comparable to the lifetimes of longer-lived features, we tend to underestimate their number. Therefore, we correct the lifetime distribution by multiplying with a weight of $(n - 2)/(n - 1 - m)$ for structures that live m frames, where n is the total number of frames. Owing to the limited spatial resolution and the finite time cadence of our observations, both distributions (lifetime and maximum area) show peaks at small values. Both distribution also have the extended tails that can be fitted with exponentials. This implies that the features do not have a characteristic lifetime or size. Their lifetimes range from <33 s (features that appear in only one frame) to 10.5 min, with $\sim 40\%$ of the features living less than 100 s. The area distribution has a peak at 0.1 arcsec^2 , with $\sim 12\%$ of the features being smaller than that. Around 97% of the features are smaller than $\sim 1 \text{ arcsec}^2$, which was given as the mean HIF size in previous studies (Ishikawa & Tsuneta 2009; Jin et al. 2009).

Figures 2c and d show scatter plots of maximum area and maximum linear polarization signal versus feature lifetime. Figure 2d has a cutoff at 0.15% , which is the lowest threshold value taken for MLT segmentation. The curves connect binned values for 189 points each. The plots indicate that longer-lasting features tend to be larger, and to display a higher mean linear polarization signal. The largest feature has a lifetime of 9.4 min and occupies up to $\sim 2.3 \text{ arcsec}^2$ in the course of its evolution. Its mean linear polarization signal reaches 0.5% .

In order to study whether the features are located in preferred locations with respect to the granular pattern, we follow the method of Lites et al. (2008). Unsharp-masked continuum images are obtained by subtracting, from the originals, the images smoothed

with a 59 pixel wide (3.2'') boxcar function. In this way, intensity variations on scales larger than granulation (due to, e.g., p-mode oscillations) are suppressed. The pixels are then sorted into 250 equally populated intensity bins, ranging from dark intergranular lanes to bright granular centers. The fractional area occupied by the HIF is calculated for each bin. The results are shown in Fig. 2e. The solid line represents unsharp-masked continuum values (see y-axis on the left). The right y-axis shows the range of fractional areas occupied by the HIF in each bin. The distribution is similar to the results shown by Lites et al. (2008, Fig. 9). It has a peak of 3.5% at positive values of the unsharp-masked intensity distribution. This suggests, as Lites et al. (2008) noticed, that HIF tend to be located at intermediate intensities, presumably at the periphery of granules.

3.2. Emergence/submergence

To estimate which percentage of the features are emerging or submerging, we study the distribution of the associated line of sight (LOS) velocities. The LOS velocities are derived from Gaussian fits to the non-reconstructed Stokes I profiles. Figure 2f shows the fractional area of the detected features associated with upflows. The distribution shows that the majority of features have a large area fraction associated with upflows. However, most of the features also have part of their area associated with downflows. Only $\sim 16\%$ of the features are fully embedded in upflows. The features fully embedded in downflows make up $\sim 8\%$ of the total number of the detected features.

Figures 2g and 2h show HIF lifetimes versus the minimum and maximum velocities, respectively, associated with the HIF during their lifetimes. Positive velocities correspond to downflows. The plots confirm that most features are associated with both up- and downflows. Moreover, the HIF tend to sample strong upflows and less strong downflows. This implies that the linear polarization signal tends to disappear before or when plasma

overturns at granule edges. Only 5% of the HIF show the stronger (> 1 km/s) downflows in intergranular lanes. Features that are fully embedded in upflows ($v_{max} < 0$) or downflows ($v_{min} > 0$) during their whole lifetime tend to be shortlived. They are also small in size (< 0.7 arcsec² for the former and < 0.3 arcsec² for the latter).

Since emerging horizontal features have been studied in some detail by other authors (Centeno et al. 2007; Martínez González & Bellot Rubio 2009; Gömöry et al. 2010), we consider here two examples of features associated with downflows. Figures 3 and 4 show the intensity pattern and LOS velocity together with the mean linear and circular polarization signals at two time instances: before and during the HIF lifetime. Overplotted contours mark the position of features detected with MLT. In Fig. 3, the continuum images show a granule at $[4'', 2.5'']$ which is fragmenting along two dark lanes. In the course of the fragmentation, one downflow lane develops while another, already existing, intergranular lane broadens. Adjacent to the granule, at the junction of the lanes being formed, a patch of stronger linear polarization signal appears at $[2.5'', 3'']$. It disappears after 2 min, when the fragmentation process finishes. The circular polarization maps show a dominant negative polarity patch at this location. A small positive patch is also visible $\sim 1''$ away from the HIF (at $[3.5'', 3'']$), at the beginning of the HIF evolution. Towards the end, the magnetic concentration of negative polarity also becomes weaker.

Figure 4 presents a similar case. The granule at $[4'', 2'']$ is fragmenting followed by the appearance of a strong downflow at the same location. Linear polarization maps show a HIF appearing in the intergranular lane, at $[3'', 2'']$, growing with time and then disappearing at the same location. During the same period, two adjacent patches of opposite polarity are visible in the circular polarization maps. The positive polarity patch increases in size, while the negative becomes weaker at the location of the downflow (at $[3'', 1'']$).

The example shown in Fig. 4 belongs to $\sim 53\%$ of the detected features that have

circular polarization signal (CP) of both polarities associated with them. The features that are associated with only one polarity (as the example shown in Fig. 3) make up $\sim 42\%$ of the total number of the detected features. The rest of the HIF has no CP higher than 2σ (0.2%) in their vicinity (in the region of ≤ 3 pixels around them). If we consider only features that are fully embedded in downflows, then $\sim 60\%$ of them are associated with only one polarity and $\sim 31\%$ is associated with CP of both polarities.

Considering results from MHD simulations, we can think of two possible scenarios for horizontal fields associated with downflows. In the first, a magnetic loop is submerged by a downflow (Stein & Nordlund 2006). In the second scenario, the field is organized in small loop-like structures and forms bundles which, observed with limited spatial resolution, appear as patches of higher linear polarization signal located in downflow lanes (Danilovic et al. 2010). As flux is being redistributed owing to the granular evolution, the bundles are dispersed and the spatial smearing of more isolated loop-like structures reduces the linear polarization signal to values below the noise level.

4. Summary

Based on Sunrise/IMaX data and using an automated detection method, we obtained statistical properties of 4536 features with significant linear polarization signal. Their lifetimes are consistent with examples given previously in the literature. However, the lifetime distribution indicates no characteristic value, in contrast to previous studies (Ishikawa et al. 2008; Ishikawa & Tsuneta 2009; Jin et al. 2009). The detected features have no characteristic size either. Around 97% of them are smaller than ~ 1 arcsec², which is the value previously taken as the mean size of HIF (Ishikawa & Tsuneta 2009). We find that their rate of occurrence is 1-2 orders of magnitude higher than reported earlier (Lites et al. 1996; Ishikawa & Tsuneta 2009; Martínez González & Bellot Rubio 2009). We

attribute this discrepancy to selection effects. If we take only the biggest features (sizes $> 0.88 \text{ arcsec}^2$), only $\sim 4\%$ of the detected features remain and the rate of occurrence decreases to $\sim 4 \cdot 10^{-5} \text{ s}^{-1} \text{ arcsec}^{-2}$, which is in closer agreement with the references cited above. Longer-lived HIF tend to be larger and display a higher mean linear polarization signals. The HIF appear preferentially at the granule boundaries, with most of them being caught by downflows at some point in their evolution. We showed that $\sim 16\%$ of the features we detected are completely embedded in upflows and $\sim 8\%$ are entirely embedded in downflows. The latter are very small in size (as illustrated by the two examples discussed in greater detail). Although their origin is still uncertain it is clear that they do not fit into the scenario of magnetic flux emergence as their physical cause.

The German contribution to *Sunrise* is funded by the Bundesministerium für Wirtschaft und Technologie through Deutsches Zentrum für Luft- und Raumfahrt e.V. (DLR), Grant No. 50 OU 0401, and by the Innovationsfond of the President of the Max Planck Society (MPG). The Spanish contribution has been funded by the Spanish MICINN under projects ESP2006-13030-C06 and AYA2009-14105-C06 (including European FEDER funds). The HAO contribution was partly funded through NASA grant number NNX08AH38G. This work has been partially supported by the WCU grant No. R31-10016 funded by the Korean Ministry of Education, Science and Technology.

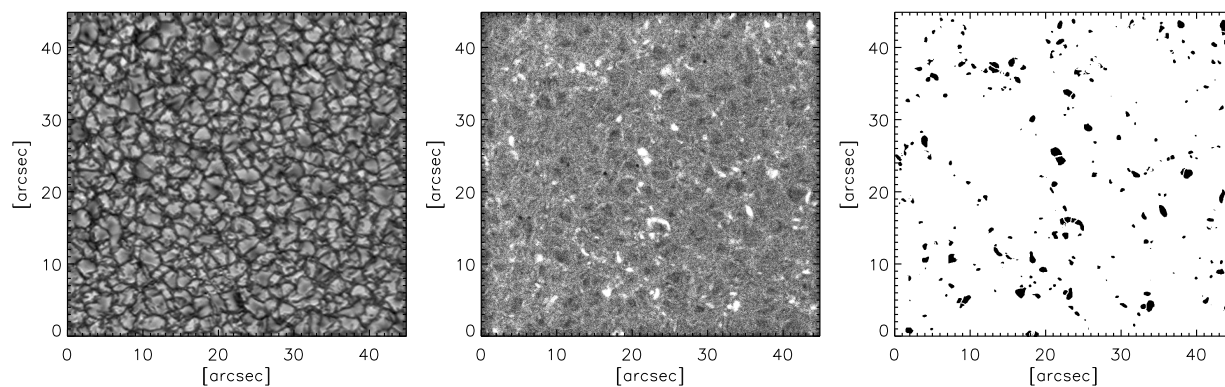


Fig. 1.— An example of a continuum intensity map (left), linear polarization map (middle) and the corresponding map of the features detected with the MLT algorithm (right). The temporal evolution of these maps (01:30:54-02:02:29 UT) is shown in the movie provided as online material (<http://www.mps.mpg.de/data/outgoing/danilovic/hif/>).

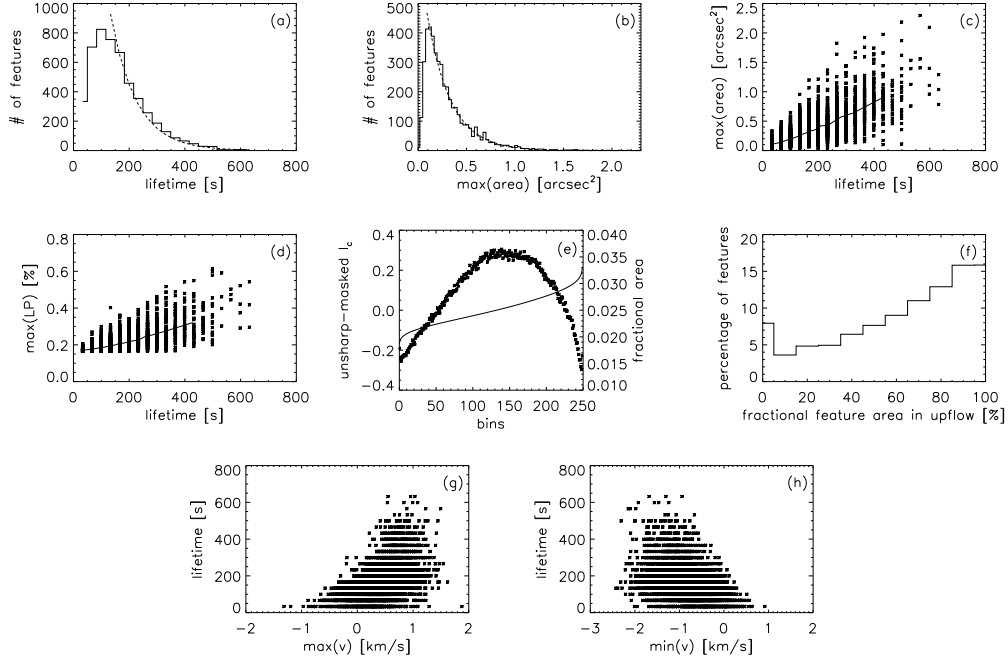


Fig. 2.— Statistical properties of detected HIF. (a) Histogram of lifetimes. The dashed line is an exponential fit with a decay time of 92 s. (b) Histogram of maximum area. The dashed line is an exponential fit with a decay scale of 0.24 arcsec². (c) Scatter plot of maximum area as a function of lifetime. (d) Scatter plot of maximum mean linear polarization signal as a function of lifetime. (e) Position of the HIF with respect to granules. The solid line indicates unsharp-masked non-reconstructed continuum intensities divided into 250 equally populated bins. The star symbols mark the fractional area of the corresponding bins occupied by the HIF. (f) Histogram of the percentage of the feature area coinciding with upflows, based on non-reconstructed LOS velocities. (g) and (h) Scatter plots of the feature lifetimes versus maximum and minimum velocity respectively associated with the detected features.

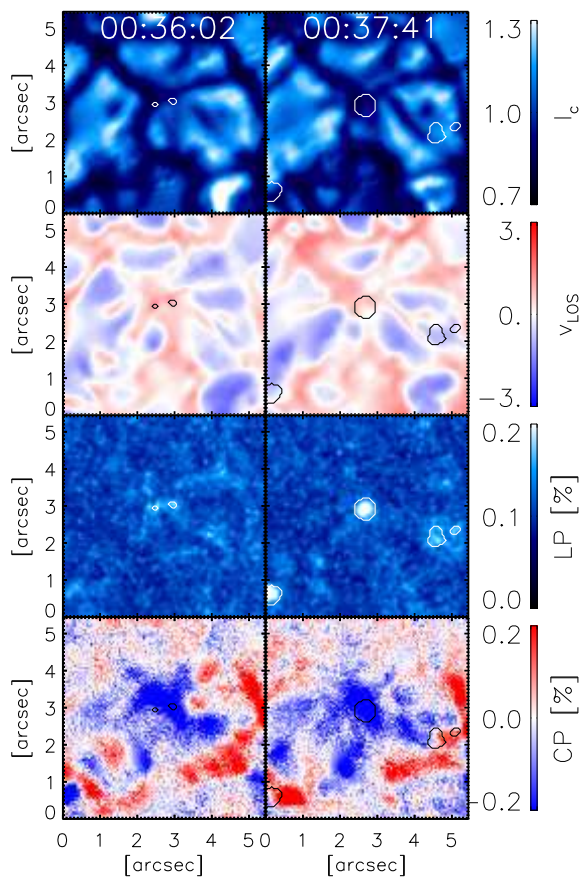


Fig. 3.— Evolution of a HIF associated with a downflow (example 1). From top to bottom: continuum intensity, LOS velocity and maps of the mean linear and circular polarization signal. The Gaussian smoothing is applied to the linear polarization map (FWHM=0.11"). Overplotted contours mark the position of the features identified with MLT. The observations were obtained at the times given in the top panels (in UT). The HIF evolution during its whole lifetime (00:36-00:40 UT) is shown in the movie provided as online material.

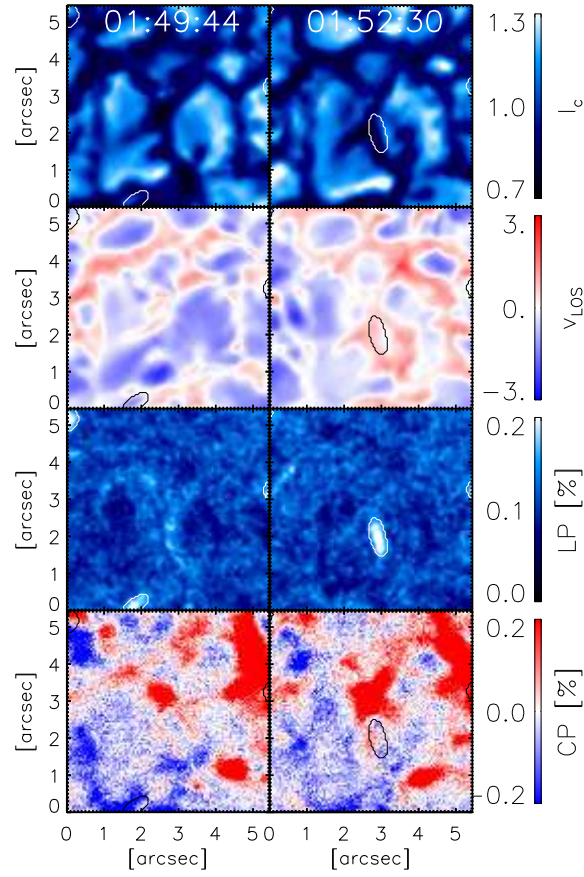


Fig. 4.— Evolution of a HIF associated with a downflow (example 2). The format is the same as in Fig. 3. The HIF evolution during its whole lifetime (01:49-01:55 UT) is shown in the movie provided as online material.

REFERENCES

- Barthol, P., Gandorfer, A., Solanki, S. K., Schüssler, M., Chares, B., et al. 2010, *Sol. Phys.*, submitted
- Berkefeld, T., Bell, A., Doerr, H. P., Feger, B., Friedlein, R., et al. 2010, *Sol. Phys.*, submitted
- Bharti, L., Beeck, B., & Schüssler, M. 2010, *A&A*, 510, A12
- Bovelet, B., & Wiehr, E. 2001, *Sol. Phys.*, 201, 13
- Centeno, R., et al. 2007, *ApJ*, 666, L137
- Cheung, M. C. M., Schüssler, M., & Moreno-Insertis, F. 2007, *A&A*, 467, 703
- Danilovic, S., Schüssler, M., & Solanki, S. K. 2010, *A&A*, 513, A1
- De Pontieu, B. 2002, *ApJ*, 569, 474
- Gandorfer, A., Grauf, B., Barthol, P., Riethmüller, T. L., Solanki, S. K., et al. 2010, *Sol. Phys.*, submitted
- Gömöry, P., Beck, C., Balthasar, H., et al. 2010, *A&A*, 511, A14
- Harvey, J. W., Branston, D., Henney, C. J., & Keller, C. U. 2007, *ApJ*, 659, L177
- Ishikawa, R., & Tsuneta, S. 2009, *A&A*, 495, 607
- Ishikawa, R., et al. 2008, *A&A*, 481, L25
- Jin, C., Wang, J., & Zhou, G. 2009, *ApJ*, 697, 693
- Kubo, M., Low, B. C., & Lites, B. W. 2010, *ApJ*, 712, 1321
- Lites, B. W., Leka, K. D., Skumanich, A., et al. 1996, *ApJ*, 460, 1019

Lites, B. W., et al. 2008, *ApJ*, 672, 1237

Martínez González, M. J., Collados, M., Ruiz Cobo, B., & Solanki, S. K. 2007, *A&A*, 469,

Martínez González, M. J., & Bellot Rubio, L. R. 2009, *ApJ*, 700, 1391

Martínez Pillet, V., et al. 2004, *Proc. SPIE*, 5487, 1152

Martínez Pillet, V., del Toro Iniesta, J. C., Álvarez-Herrero, A., Domingo, V., Bonet
Navarro, J. A., et al. 2010, *Sol. Phys.*, submitted

Orozco Suárez, D., Bellot Rubio, L. R., & del Toro Iniesta, J. C. 2007, *ApJ*, 662, L31

Orozco Suárez, D., et al. 2007, *ApJ*, 670, L61

Schüssler, M., & Vögler, A. 2008, *A&A*, 481, L5

Solanki, S. K., Barthol, P., Danilovic, S., Feller, A., Gandorfer, A., et al. 2010, *ApJ*, this
volume

Stein, R. F., & Nordlund, Å. 2006, *ApJ*, 642, 1246

Steiner, O., Rezaei, R., Schaffenberger, W., & Wedemeyer-Böhm, S. 2008, *ApJ*, 680, L85